BioChem

MDPI

Review

Advancements in Retinal Tissue-Mimicking Optical Coherence Tomography Phantoms: Materials, Properties, and Applications

Mukhit Kulmaganbetov [1,2,3]

[1] Centre for Eye and Vision Research (CEVR), 17W Hong Kong Science Park, Hong Kong; mukhit.k@cevr.hk
[2] School of Optometry and Vision Sciences, Cardiff University, Cardiff CF24 4HQ, UK
[3] Kazakh Eye Research Institute, Almaty A05H2A8, Kazakhstan

Abstract: Optical coherence tomography (OCT) phantoms are essential tools for calibrating imaging systems, validating diagnostic algorithms, and bridging technological advancements with clinical applications. This review explores the development and application of materials used in OCT phantoms, emphasising their optical, mechanical, and biochemical fidelity to biological tissues. Gelatin-based phantoms (n = 1.35) offer controllable absorbance and scattering, with penetration depths (PDs) of 500–2000 µm and scattering coefficients (SCs) of 5–20 cm^{-1} but are unstable at room temperature. Silicone phantoms (n = 1.41) are durable and stable, with SCs of 10–15 cm^{-1}, suitable for long-term studies. Polydimethylsiloxane (PDMS) phantoms (n = 1.41) provide manageable optical properties and are used in microfluidic applications. Polyvinyl alcohol (PVA) phantoms (n = 1.48) mimic soft tissue mechanics, with SCs of 5–15 cm^{-1}, but require freeze–thaw cycles. Fibrin phantoms (n = 1.38) simulate blood clotting, with SCs of 5–20 cm^{-1}. Scattering particles like polystyrene (n = 1.57) and titanium dioxide (TiO_2, n = 2.49) offer modifiable properties, while silica microspheres (SiO_2, n = 3.6) and gold nanoshells (n = 2.59) provide customisable optical characteristics. These materials and particles are crucial for simulating biological tissues, enhancing OCT imaging, and developing diagnostic applications. Despite progress, challenges persist in achieving submicron resolution, long-term stability, and cost-effective scalability.

Keywords: optical coherence tomography; phantom; scattering

Academic Editor: Buyong Ma

Received: 13 February 2025
Revised: 3 April 2025
Accepted: 7 April 2025
Published: 9 April 2025

Citation: Kulmaganbetov, M. Advancements in Retinal Tissue-Mimicking Optical Coherence Tomography Phantoms: Materials, Properties, and Applications. *BioChem* **2025**, *5*, 6. https://doi.org/10.3390/biochem5020006

1. Introduction

Over the past two decades, while OCT technology has advanced rapidly, the development of standardised test methods to evaluate its functionality has lagged behind. Phantoms are artificial models essential for assessing imaging devices, maintaining signal quality over time, and facilitating comparisons between different devices [1].

The materials used in phantom preparation for various imaging techniques, such as ultrasound [2], optical spectroscopy, imaging, and dosimetry [3], are diverse. These materials are designed to emulate the specific biological and optical properties of tissues. Additionally, phantoms can mimic cellular and subcellular structures by matching the size, refractive index, and volume of scatterers, as well as the matrix medium. These biological structures can be as small as a micron or less.

In the context of retinal neurodegenerations, such as glaucoma and age-related macular degeneration, apoptosis of retinal ganglion cells (RGCs) and photoreceptors is an early pathological event [4–7]. To detect early, subtle cellular and subcellular changes associated with cell death, phantoms can be created using microparticles sized 1–3 microns, which

correspond to the dimensions of organelles like mitochondria, the Golgi apparatus, and the endoplasmic reticulum [8–10]. These phantoms can replicate organelle morphology and are useful for exploring the resolution capabilities of OCT systems and training machine learning tools for OCT-based retinal detection [11].

Optical phantoms are indispensable for evaluating imaging systems, and their design has evolved significantly with the introduction of advanced materials. Recent advancements in OCT phantom development emphasise the use of materials like polydimethylsiloxane (PDMS) and hydrogels doped with nanoparticles to simulate multi-layered retinal structures. This enables precise calibration of axial resolution and depth-dependent imaging performance [12]. High-resolution 3D printing can replicate micrometre-scale anatomical features, such as layered photoreceptors and capillary networks, improving the benchmarking of OCT systems [13]. Agrawal et al. (2020) demonstrated the use of an engineered texture phantom with biologically inspired microfeatures to quantitatively assess lateral resolution in adaptive optics (AO) systems, providing a standardised approach for evaluating retinal imaging performance [14].

This paper reviews the materials used to prepare OCT retinal phantoms, focusing on their optical and mechanical properties, advantages, disadvantages, and potential applications. It concludes by addressing the ongoing challenges in selecting phantom materials, their preparation, and their application in OCT diagnostics, highlighting areas for future research.

The commonly used materials for the matrix media and scattering particles in OCT phantoms are detailed here. The matrix medium simulates the cytoplasm and intercellular matrix, while the scatterers represent dense particles of cellular morphology, including cell and nuclear membranes and organelles (Figure 1). Tables 1 and 2 summarise the phantom matrices and scattering particles, respectively, their optical and mechanical properties, and the advantages and disadvantages of phantom preparation.

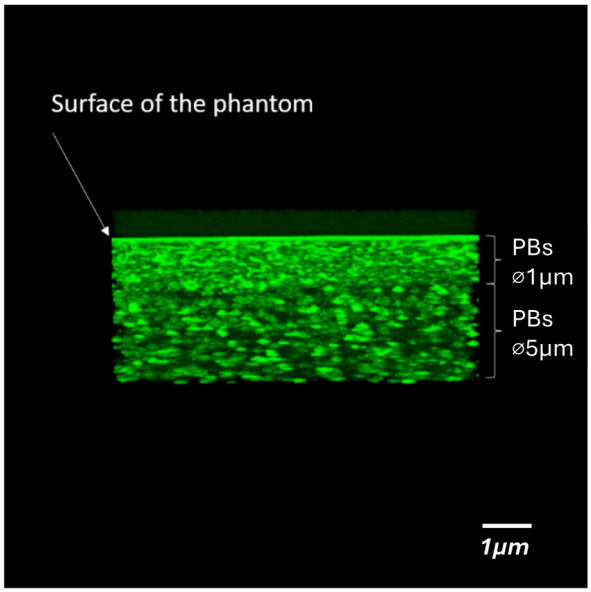

Figure 1. Rendered optical coherence tomography (OCT) image of bilayer phantom with gelatin-based matrix and polystyrene beads (PBs) as a scattering particle. The upper layer contains 1 μm diameter PBs, whereas the bottom layer consists of PBs with 5 μm diameter. The image was acquired using a custom-built OCT system with centre λ = 1040 nm (FWHM = 70 nm) at the Cardiff University School of Optometry and Vision Sciences. Preparation and imaging of the OCT phantoms can be found in our previous study [11].

Table 1. Summary of phantom matrices.

Substances	RI	Advantages	Disadvantages	PD, μm	SC, cm^{-1}	AC, cm^{-1}	MS, MPa	DT	Applications
Gelatin-based phantoms	1.35	• controllable absorbance and scattering • background fluorescence • optical and mechanical properties close to biological tissue • cost-effectiveness	• unstable at room temperature • difficult to make complex shapes and forms	500–2000	5–20	0.1–1	0.01–0.1	days to weeks	• simulate soft biological tissues • calibration and testing of OCT systems • educational settings to demonstrate imaging techniques
Silicone phantoms	1.41	• rupture resistance and stable • easy to make complex shapes and forms	• inhomogeneous with inorganic particles (fluorophores, chromophores and absorbers) • inconsistent with biological and organic constituents	1000–2000	10–15	<1	0.1–3	years	• used for their durability and stability, making them suitable for long-term studies and repeated use • development and testing of medical imaging devices
Polydimethylsiloxane (PDMS) phantoms	1.41	• manageable optical properties • compatible with inorganic particles • long-term durability and stability	• hard to work with hydrophilic chromophores and scatterers	1000–2000	5–10	<0.1	0.5–3	years	• in microfluidic applications and in the study of vascular structures • visualising and analysing flow dynamics and structural imaging
Polyvinyl alcohol (PVA) phantoms	1.48	• similar to extracellular liquid physical properties • longevity • rigid structure • inexpensiveness	• difficult to control optical properties • dependent to freeze and thaw cycles	1000–2000	5–15	<1	0.01–1	months to years	• mimic the mechanical properties of soft tissues • calibration of elastography techniques and in the development of surgical training models

Table 1. *Cont.*

Substances	RI	Advantages	Disadvantages	PD, μm	SC, cm^{-1}	AC, cm^{-1}	MS, MPa	DT	Applications
Fibrin phantoms	1.38	• works well with organic and inorganic particles • low scattering coefficient	• time-consuming phantom preparation	1000–2000	5–20	<1	0.001–0.01	days to weeks	• simulate blood clotting and vascular structures

Abbreviations: AC—absorption coefficient; DT—degradation time; MS—mechanical stiffness (Young's Modulus); PD—penetration depth; RI—refractive index; SC—scattering coefficient.

Table 2. Summary of scattering particles.

Substances	RI	Advantages	Disadvantages	SC, cm^{-1}	AC, cm^{-1}	MS, GPa	Applications
Polystyrene	1.57	• modifiable mechanical and optical properties • available in various sizes	• high-priced • the short lifespan of the phantoms	50–100	<0.01	3–3.5	• simulate the scattering properties of biological tissues • precise control over the scattering characteristics of the phantom (wide range of sizes) • calibrating and testing the resolution and sensitivity of OCT systems
Titanium dioxide (TiO_2)	2.49	• cost-effectiveness • availability	• inhomogeneous phantom if solid • short lifespan • hard to control optical properties	100–200	<0.1	230–280	• mimic the high scattering properties of certain tissues (skin or fibrous tissues) • studies focused on improving image contrast and depth penetration in OCT imaging
Silica microspheres (SiO_2)	3.6	• customizable optical properties • large scattering cross-section	• unavailability	50–150	<0.01	70–75	• employed in phantoms designed to simulate the optical properties of various tissues, including brain and muscle tissues • multi-modal imaging studies
Gold nanoshells	2.59	• controllable optical properties • compatible with biological tissue	• high-priced • unavailability	50–150	1–10	70–80	• research focused on photothermal therapy and contrast-enhanced OCT imaging

Abbreviations: AC—absorption coefficient; MS—mechanical stiffness (Young's Modulus); RI—refractive index; SC—scattering coefficient.

2. Phantom Matrix

The phantom matrix serves as the artificial medium that replicates the intracellular space and cytoplasm of tissues. Therefore, its physical and chemical properties should closely resemble those of the fluid compartments found in tissues and cells, such as intracellular fluid and cytoplasm. In addition to the matrix, OCT phantoms incorporate chemicals with higher refractive indices and specific sizes and shapes, which act as scatterers for OCT light. These scatterers simulate the cell and nuclear membranes, as well as organelles. Below, we define the materials commonly used as phantom matrices.

2.1. Gelatin-Based Phantoms

Gelatin, a homogeneous colloid gel derived primarily from animal collagen [15], is one of the earliest materials used for phantom preparation, alongside other hydrogel-based substances like agarose [16,17]. These organic materials are well-characterised and easily controlled. Alimentary gelatin and agar are readily available, exhibiting minimal absorption and very low turbidity [18].

As a matrix for phantoms, gelatin encapsulates water as its main component and can be combined with both organic and inorganic scattering particles to mimic the heterogeneous structure of tissues [19–21]. Gelatin's optical and mechanical properties are relatively similar to those of biological tissues [22]. For example, its mechanical properties, such as wave speed (in ultrasonography) and mass density (approximately 1000 kg/m^3), align closely with those of tissue [23].

In a study by Zhang et al. (2011), elasticity measurements of five phantoms with varying gelatin concentrations demonstrated a positive correlation between elasticity and gelatin concentration [24]. The refractive index of a gelatin phantom is 1.35, which is close to that of biological materials, and its scattering coefficient is 1 at a central wavelength of 1280 nm, as calculated by Mie theory [22]. Consequently, gelatin-based matrices possess the desired absorbance, scattering, and background fluorescence for creating tissue-mimicking optical phantoms. Additionally, the optical properties, particularly the variation in transmission at wavelengths of 600–1000 nm, remain stable for 2–4 weeks [25], making them suitable for a series of phantom fabrication and imaging studies.

The scattering and absorption properties of gelatin phantoms can be adjusted by mixing the gelatin medium with a lipid emulsion [18,26]. In this combination, the lipid emulsion enhances absorption and fluorescence, while gelatin provides rigidity and scattering characteristics [15,27]. However, gelatin-based phantoms lack rigidity at room temperature, which limits their durability and complicates the creation of complex shapes and forms [28]. Due to gelatin's lower viscosity (<2 Pa) compared to tissue, its elasticity is sensitive to fabrication, testing, and imaging conditions [29]. Like other hydrogels, gelatin's stiffness restricts water mobility, but additives such as EDTA, penicillin, fluorophores, gadolinium, and copper sulphate can enhance the functionality of gelatin-based phantoms [3].

Given these optical and mechanical properties and its availability, gelatin is a common foundational material for tissue-imitating phantoms used in evaluating diagnostic equipment and software. Furthermore, gelatin-based phantoms are cost-effective, making them valuable for training and practical applications [30].

2.2. Silicone Phantoms

Silicone offers the ability to create phantoms with complex shapes and diverse optical properties, addressing some of the limitations associated with gelatin-based phantoms. This is due to silicone's low viscosity and resistance to fracture, which also allow for the creation of permanent phantom media suitable for routine testing and calibration of devices. The refractive index of silicone is approximately 1.4 [31], closely matching the average

value for human tissue [32] and the retina [33]. Silicone's scattering contribution is minimal, with an attenuation coefficient of less than 0.5 mm^{-1} [34].

As a matrix for phantoms, silicone is both stable and transparent, making it suitable for a wide range of scattering particles. However, achieving a homogeneous distribution of inorganic scatterers, such as fluorophores, chromophores, and absorbers, can be challenging. Bays et al. (1997) addressed this by adding solvents like water, ethanol, methanol, and dimethyl sulfoxide to silicone-based phantoms to create a solution with scattering particles [32]. After mixing with silicone, the solvents were removed through evaporation, resulting in a monodispersed distribution of scattering particles within the matrix [32].

Silicone-based phantoms are also useful for measuring blood flow velocity in Doppler OCT [35]. This can be achieved by embedding a flow channel with a diameter of 50–150 µm, similar to retinal vessels, within an eye model. Phantoms incorporating special gel colourants for silicone and TiO_2 scatterers can be employed to investigate both relative changes and absolute values of retinal blood flow velocity [36].

Despite these advantages, silicone has some drawbacks as a phantom material, notably its incompatibility with biological tissue constituents and other organic chemicals [3]. Significant efforts have been made to develop silicone-based optical phantoms, promoting the use of polymeric organosilicon, such as polydimethylsiloxane (PDMS).

2.3. Polydimethylsiloxane Phantoms

The use of PDMS, a silicon-based elastomeric polymer, in phantom preparation is increasingly popular. PDMS is optically transparent, with a refractive index of 1.41 ± 0.01 in the near-infrared range (λ = 800–1300 nm) [1]. Its optical properties can be precisely controlled to achieve various intensity levels [37,38]. Inorganic scatterers can be incorporated to mimic tissue structures with similar absorption and scattering coefficients [39]. However, due to PDMS's hydrophobic nature, hydrophilic chromophores and scatterers cannot be used, which is a limitation of this polymer.

PDMS maintains its stability over long periods, lasting several years [40]. The fabrication of PDMS phantoms is straightforward, as well as easy and safe to use [41]. Mixing silicone with PDMS allows for customizable viscosity, although the softening process of silicone can take weeks to cure if not heated [28]. Once cured, the elastic polymer is strong and retains consistent optical properties, as demonstrated in the study by Wu et al. (2015) [42].

Thanks to its tunable optical properties, PDMS is suitable for creating multi-layered phantoms [43]. Baxi et al. (2014) used PDMS as a matrix for phantoms, adding scatterers such as barium sulphate ($BaSO_4$) powder, titanium dioxide (TiO_2) nanopowder, and silica (SiO_2) microspheres [1]. These substances were varied in concentration across layers to mimic different retinal layers. A spin-coating method was employed to achieve similar thickness and intensity for each retinal layer [1].

Wang et al. (2021) developed a custom-built eye model with PDMS and polystyrene bead-embedded phantoms for the calibration and quality assessment of OCT devices [44], including evaluating the axial and lateral resolution of tomography. The potential of PDMS extends to retina-mimicking phantoms and can be used for fabricating external eye structures [45] and preparing birefringent tissue phantoms (such as the cornea and retina), which can be imaged using polarisation-sensitive OCT [46].

2.4. Polyvinyl Alcohol (PVA) Phantoms

Polyvinyl alcohol (PVA) has been introduced as a phantom matrix material to enhance the quality of artificial tissues [2,47], particularly in ultrasound, photoacoustic tomography, and MRI research [48,49]. PVA is a synthetic polymer that can form a hydrogel when

dissolved in water or dimethyl sulfoxide (C_2H_6OS). Following freeze/thaw processes, this solid composition is known as PVA-cryogel (PVA-C) [28].

The mechanical properties of PVA-C closely resemble those of human tissue [50,51], exhibiting increased inherent breaking strength after freeze–thaw cycles and elastic characteristics similar to the extracellular matrix [49]. Although PVA's mechanical properties are tunable, controlling its scattering features is challenging [3]. The optical properties depend on additives, catalysts, water, and C_2H_6OS [28]. Additionally, the scattering coefficient can be adjusted through repeated freeze and thaw cycles; for example, after seven cycles, the scattering coefficient decreases to 0.8–1 mm [52].

An innovative application of PVA as an ophthalmic phantom was demonstrated by Fogli et al. (2014), who used the polymer as a synthetic vitreous humour for vitrectomy procedures [53]. The rigid structure, cost-effectiveness, and long-term durability of PVA-C make it a promising material for retinal and vitreous phantoms, facilitating the evaluation of optical diagnostic and surgical devices.

2.5. Fibrin Phantoms

Fibrin overcomes many of the disadvantages associated with other phantom materials. As a natural protein, fibrin provides structural support in biological tissues, particularly in blood clots. It forms when fibrinogen is activated by the proteolytic action of thrombin [54]. Fibrin is transparent and can be combined with both inorganic and organic chemicals to enhance the scattering coefficient of the resulting phantom. Additionally, fibrin is compatible with biological tissues and hydrogels [28].

The process of preparing fibrin phantoms is straightforward and not time-consuming. The primary components needed are fibrinogen and thrombin, with their concentrations affecting the mechanical properties of the phantom [55]. Kennedy et al. (2010) demonstrated the creation of a fibrin phantom combined with Intralipid™ [56]. The low scattering characteristic of fibrin makes it an excellent choice for a phantom matrix in OCT devices, while Intralipid serves as the scatterer to mimic cell and organelle membranes [3]. The inclusion of these lipid scattering materials allows for precise control over the optical properties. Another example of using fibrin with Intralipid in a phantom was presented by Yu et al. (2014), showcasing a time-efficient fabrication process and an extended phantom lifespan with low scattering ($\mu's = 1.25 \pm 0.04\ mm^{-1}$) [57].

Newer materials such as agarose [58], polyethylene glycol diacrylate (PEGDA) [59], and alginate hydrogels [60,61] are increasingly used in phantom fabrication due to their advantageous optical and mechanical properties. Agarose hydrogels, with a refractive index similar to gelatin, provide low turbidity and can be adjusted for varying optical densities, making them suitable for optical applications [58]. They are easy to prepare and form stable structures at room temperature, offering moderate mechanical strength, often enhanced by combining with other materials. PEGDA hydrogels are highly transparent and can be engineered to have specific refractive indices by varying polymerization conditions, making them ideal for phantoms with precise optical properties: tunability and biocompatibility [59]. Known for their biocompatibility, alginate gels have adjustable mechanical properties and are particularly useful in organ-on-chip models, with stability enhanced through crosslinking with calcium ions [62]. These materials provide versatile options for developing phantoms that closely mimic biological tissues in both optical and mechanical aspects.

3. Scattering Particles

In addition to the medium material, phantoms incorporate scattering constituents, which enable precise and independent control of optical properties. Phantoms can be cate-

gorised into two main groups based on how their light scattering properties are achieved: those using nano- or microparticle-induced scattering and those relying on the intrinsic scattering of the materials used. The type, size, shape, and concentration of scatterers are crucial in achieving the desired scattering coefficient for phantoms.

3.1. Polystyrene

Polystyrene beads are among standard optical phantoms' most commonly used scattering particles [3]. These microspheres offer easily controllable physical and optical properties, and their refractive index can be adjusted [63]. The size and concentration of the beads significantly influence their optical scattering properties [64], with a scattering coefficient of 2.3 and a refractive index of 1.59 [22]. The availability of beads in various sizes and refractive index is another advantage, allowing for good repeatability and theoretical prediction of spectra [3]. Like other polymer beads, polystyrene is suitable for assembling multilayer phantoms. Chang et al. (2012) used layered phantoms with polystyrene microspheres to assess and validate OCT axial resolution and depth of field [65]. Scanning electron microscopy (SEM) images reveal the uniformity and spherical shape of polystyrene beads, contributing to their predictable scattering behaviour.

Due to their unique optical properties, including a tunable scattering coefficient and refractive index, polystyrene beads are often the first choice for OCT phantom preparation. In gelatin-based phantoms, polystyrene nanoparticles are frequently used as scattering constituents. However, because of the cost and short lifespan of these phantoms (ranging from 1 day to 1 week, rarely longer), alternatives such as titanium dioxide (TiO_2) and aluminium oxide (Al_2O_3) powders are often preferred.

3.2. Titanium Dioxide

Titanium dioxide (TiO_2) is a widely used particle mixture in optical phantoms due to its high scattering coefficient and low absorption value, with peak absorbance occurring at wavelengths of 250–450 nm [3,66]. For well-defined and reproducible optical properties, it is preferable to use liquid-based supplies of TiO_2, as the powder form requires continuous stirring to achieve a homogeneous phantom with a solid dispersion of scatterers [67].

TiO_2, along with other inorganic scattering materials like aluminium oxide (Al_2O_3) or barium oxide (BaO), is ideal for gelatin-based phantoms because of its availability and cost-effectiveness. However, like gelatin, TiO_2 has a limited lifespan, which restricts its use in phantoms over time. Achieving an exact scattering coefficient from a phantom mixture can be challenging, as demonstrated by Pogue and Patterson (2006), who reported significant variability in scattering from TiO_2 phantoms [3].

The effective resolution of a speckle-modulating OCT (SM-OCT) system was enhanced by imaging a small gap in a PDMS-based phantom containing a titanium dioxide mixture [68]. Compared to other scatterers, TiO_2 has a higher refractive index, making it suitable for mimicking the hyperreflective retinal pigment epithelium and photoreceptors [1]. In the wide-field eye phantom developed by Corcoran et al. (2015), TiO_2 was a key component of the Verowhite region, used to design concentric rings of high-scattering materials, while carbon black served as Veroblack to increase absorption [69].

Beyond SD-OCT and SM-OCT, TiO_2 is also used in the preparation of retinal phantoms for OCT-angiography [70], for fabricating microfluidic channels, and in adaptive optics (AO) OCT [14] to replicate the opto-structural properties of photoreceptor outer segments [71]. Kuttippurath et al. (2023) demonstrated the utility of TiO_2-doped gel wax phantoms to replicate lipid absorption features at 1210 nm, validating a 1200 nm spectroscopic OCT system's ability to discriminate lipid-rich tissues from water-based environments using attenuation spectral analysis and predictive modelling [72]. These

lipid-mimicking phantoms are particularly valuable for studying diseases like AMD, where lipid dysregulation in the retinal pigment epithelium (RPE) is a hallmark [73].

3.3. Silica Microspheres

Silica microspheres (SiO_2) offer low to moderate levels of OCT signal intensity compared to titanium dioxide [1], yet they have a relatively high refractive index of about 3.6 in the red and near-infrared spectral regions [74]. The first silicone-based phantom using silica microspheres as scatterers was developed by Charles-Etienne et al. (2008), who demonstrated the relationship between speckle size in OCT and the density of microspheres [75]. SiO_2 maintains a simple, well-defined microstructure and has a sufficiently large scattering cross-section. Additionally, silica nanoparticles facilitate elastography due to a speckle field pattern that can be easily tracked [75].

SEM images show well-defined microstructures of SiO_2, contributing to their large scattering cross-section. Silicon nanoparticles (SiNPs) are gaining attention due to their unique optical properties and biocompatibility. Recent studies have explored the use of these particles in enhancing OCT contrast [76], although comprehensive validation studies are still needed.

The preparation methods for silica microspheres vary and include techniques such as laser ablation and electrochemical etching followed by mechanical grinding [77]. The choice of method depends on the desired target size of the SiO_2 for OCT phantoms.

3.4. Gold Nanoshells

Gold nanoshells are emerging as a promising scattering particle for optical imaging techniques [78]. These nanostructured particles consist of a dielectric core surrounded by a gold shell. By adjusting the parameters of this core/shell structure, the wavelength can be tuned to match the surface resonance [79].

Agrawal et al. (2006) demonstrated that the optical properties of phantoms depend on the concentration of gold nanoshells [80]. Higher concentrations of nanoshells enhance the OCT signals backscattered from tissue [81]. The scattering strength of these particles is sufficient to mimic biological tissue in phantoms and even skin in vivo [82]. In initial experimental models, OCT signal enhancement reached 7 dB [83]. Tuersun et al. (2015) studied the optimal dimensions of nanoparticles to achieve the maximum scattering coefficient (7.01 μm^{-1}), determining that a core radius of 54.2 nm and a gold shell thickness of 10.1 nm at a wavelength of 830 nm were ideal [79]. SEM images of gold nanoshells show their unique core–shell structure [84], which is critical for their optical behaviour.

In addition to their use in imaging, gold nanostructured particles are also being explored as a treatment option for photothermal therapy of cancer, thanks to their high absorption in the near-infrared region and favourable thermal characteristics [79].

4. Molecular Mechanisms in OCT-Studied Retinal Diseases

Recent advances in OCT have enabled the correlation of structural retinal changes with molecular pathways. Below, we highlight key biochemical mechanisms studied using OCT, emphasising their relevance to phantom design for disease modelling.

4.1. Lipid Metabolism and RPE Dysfunction

Progressive rod-cone degeneration (PRCD)-deficient mice exhibit aberrant lipid accumulation in the retina, including elevated cholesteryl esters and lipofuscin deposits in the RPE, mimicking age-related macular degeneration (AMD) pathology. These lipid-driven changes correlate with OCT-detected hyperreflective RPE lesions and Bruch's membrane deposits [73]. Phantoms replicating lipid-rich environments (e.g., using TiO_2-doped matrices) are critical for validating OCT systems in detecting early AMD biomarkers [72,73].

While oxidative stress is theorised to contribute to vitreomacular interface pathologies like epiretinal membranes (ERMs), recent OCT studies found no correlation between total oxidant status in surgically removed ERMs and retinal morphological changes [85]. This highlights the need for phantoms incorporating reactive oxygen species (ROS)-responsive nanoparticles to better model oxidative stress dynamics in vitro.

4.2. Complement System in Photoreceptor Degeneration

C3 knockout mice show reduced photoreceptor loss in sodium iodate-induced retinal degeneration models, implicating complement-mediated outer segment opsonisation in disease progression [86]. OCT phantoms with tunable scattering properties (e.g., gold nanoshells) can simulate complement-driven structural changes to optimise therapeutic monitoring.

4.3. Lysosomal Storage Disorders and Phagocytosis Defects

CLN3 disease models demonstrate impaired RPE phagocytosis of photoreceptor outer segments, leading to lipofuscin accumulation and photoreceptor loss visible on OCT [87]. Multi-layered PDMS phantoms with lipid-rich scatterers can emulate these defects to test OCT-based diagnostic algorithms.

A porcine retinal hole model demonstrated that holes < 1380 µm close via astrocyte-dominated gliotic plug formation visible on OCT [88]. Phantoms with PDMS-based glial cell mimics could help calibrate OCT systems to track wound healing responses in macular hole surgery.

Validating phantoms against in vivo OCT data involves a comparative analysis of OCT signals from phantoms and in vivo tissues [89], assessing parameters such as signal intensity, scattering profiles, and structural resolution. Key metrics used in validation include the scattering coefficient, signal-to-noise ratio (SNR), and axial and lateral resolution, ensuring that phantoms exhibit similar optical behaviour and image quality as biological tissues. For instance, phantoms designed to mimic AMD incorporate lipid-rich environments to replicate drusen deposits, with validation comparing OCT signal intensity and scattering profiles to in vivo AMD lesions.

5. Discussion

The advancement of OCT technology focuses on several key areas: enhancing axial and lateral resolutions and penetration through improved light sources, implementing adaptive optics for isotropic resolution, and applying AI-based tools for image classification. Despite significant progress in these areas over the past two decades, there has been limited development in standard test methods to assess the performance of OCT devices. Phantoms serve as essential test models for ensuring the quality of OCT hardware and software, as well as for dynamic quality control and device comparison, maintaining reliability and accuracy in medical diagnostics.

Most commercial phantoms are made from hard plastics and are used to validate clinical machines such as computed tomography, ultrasound, magnetic resonance imaging, biomedical optical spectroscopy, Raman spectroscopy, OCT, and near-infrared fluorescence [27]. Heikka et al. (2020) conducted a comparison of commercially available phantoms across eleven OCT machines, demonstrating highly comparable outcomes when the data were analysed consistently [90]. The adoption of PDMS and hydrogels addresses key challenges in phantom fabrication, such as achieving anatomical accuracy in retinal layers while maintaining optical stability [15].

One of the main limitations of titanium and silicon dioxides is their tendency to aggregate, which can affect their dispersion. In the case of TiO_2, their high surface energy

and reactivity can lead to aggregation when exposed to certain conditions, such as changes in pH, temperature, or solvent composition. This aggregation can result in the formation of larger clusters or agglomerates, which may impact the uniformity and stability of the dispersion. Similarly, SiO_2 particles also face challenges related to aggregation and dispersion. The surface properties of SiO_2 particles can influence their interaction with surrounding molecules or particles, leading to agglomeration. This agglomeration can hinder the effective dispersion of SiO_2 particles in a matrix medium.

Addressing the challenges of OCT imaging through mediums like silicon oil or gas involves understanding their optical properties and developing phantoms that simulate their effects on image quality. Silicon oil, with a refractive index of n = 1.40, can create significant refractive index mismatches when used as a tamponade in the eye, leading to image distortion, reduced resolution, and artefacts in intraoperative OCT [91]. Similarly, gases used in ophthalmic procedures, such as perfluoropropane (C_3F_8) [92] or sulphur hexafluoride (SF6) [93], have much lower refractive indices compared to biological tissues, resulting in altered light paths and reduced image clarity. Both silicon oil and gas can alter the scattering properties of the medium, affecting the OCT signal's intensity and contrast and complicating the interpretation of structural details. To address these challenges, phantoms can be designed using materials that closely match the refractive index of silicon oil or gas, incorporating layered structures to simulate the interface between biological tissues and these mediums.

Tissue phantoms with anatomically realistic geometries face limitations because they simulate tissue on a large spatial scale but do not adequately capture the complex optical absorption and scattering properties arising from cellular, subcellular, and tissue structures of varying sizes. Zhang et al. (2024) recently demonstrated that high-resolution 3D printing enables the creation of retinal phantoms with micrometre-scale anatomical features, including layered photoreceptors and capillary networks, which closely match human retinal morphology and improve OCT system benchmarking [13].

Recent studies demonstrate that OCT-detected structural alterations often correlate with molecular dysfunction. For instance, lipid-rich TiO_2 phantoms replicate drusen-like deposits in AMD, which are associated with PRCD gene mutations and oxidative stress in the RPE [73,85]. Similarly, PDMS-based multi-layered phantoms with tunable scattering coefficients can model complement-mediated photoreceptor degeneration observed in sodium iodate-treated retinas [86], providing testbeds for anti-complement therapies. These applications underscore the importance of matching phantom material properties (e.g., refractive index, scattering coefficients) to the biochemical signatures of diseases.

Ensuring the consistency and reliability of phantoms across different studies and applications can be achieved by standardisation procedures. The National Institute of Standards and Technology (NIST) has been involved in developing reference materials and protocols for the characterisation of optical phantoms. These efforts aim to provide benchmarks for optical properties, such as scattering and absorption coefficients, ensuring that phantoms used in research and clinical practice meet consistent quality standards [94].

The development of multimodal phantoms represents a promising frontier in medical imaging. By integrating OCT with fluorescence and photoacoustic imaging, these phantoms can provide a more comprehensive understanding of biological tissues and disease processes. Future research should focus on material innovation, dynamic simulation, and standardisation to fully realise the potential of multimodal phantoms in advancing medical diagnostics and improving patient outcomes.

Phantoms with well-defined optical and mechanical properties can be used to generate training data for artificial intelligence (AI) models. These models can then be applied to OCT images to improve the detection and classification of retinal diseases. In our recent study,

we demonstrated the use of phantoms in training machine learning tools for OCT-based retinal detection [11], highlighting their role in advancing AI-driven diagnostics [95–97].

Funding: M.K. was supported by a scholarship from the Cardiff University Vice-Chancellor's International Scholarships for Research Excellence, the InnoHK initiative of the Innovation and Technology Commission of the Hong Kong Special Administrative Region Government.

Conflicts of Interest: The author declares no conflicts of interest.

References

1. Baxi, J.; Calhoun, W.; Sepah, Y.J.; Hammer, D.X.; Ilev, I.; Pfefer, T.J.; Nguyen, Q.D.; Agrawal, A. Retina-simulating phantom for optical coherence tomography. *J. Biomed. Opt.* **2014**, *19*, 021106. [CrossRef] [PubMed]
2. Culjat, M.O.; Goldenberg, D.; Tewari, P.; Singh, R.S. A review of tissue substitutes for ultrasound imaging. *Ultrasound Med. Biol.* **2010**, *36*, 861–873. [CrossRef]
3. Pogue, B.W.; Patterson, M.S. Review of tissue simulating phantoms for optical spectroscopy, imaging and dosimetry. *J. Biomed. Opt.* **2006**, *11*, 041102. [CrossRef]
4. Dunaief, J.L.; Dentchev, T.; Ying, G.S.; Milam, A.H. The role of apoptosis in age-related macular degeneration. *Arch. Ophthalmol.* **2002**, *120*, 1435–1442. [CrossRef]
5. Vernazza, S.; Oddone, F.; Tirendi, S.; Bassi, A.M. Risk Factors for Retinal Ganglion Cell Distress in Glaucoma and Neuroprotective Potential Intervention. *Int. J. Mol. Sci.* **2021**, *22*, 7994. [CrossRef] [PubMed]
6. Williams, P.A.; Howell, G.R.; Barbay, J.M.; Braine, C.E.; Sousa, G.L.; John, S.W.; Morgan, J.E. Retinal Ganglion Cell Dendritic Atrophy in DBA/2J Glaucoma. *PLoS ONE* **2013**, *8*, e72282. [CrossRef]
7. Williams, P.A.; Thirgood, R.A.; Oliphant, H.; Frizzati, A.; Littlewood, E.; Votruba, M.; Good, M.A.; Williams, J.; Morgan, J.E. Retinal ganglion cell dendritic degeneration in a mouse model of Alzheimer's disease. *Neurobiol. Aging* **2013**, *34*, 1799–1806. [CrossRef] [PubMed]
8. Beuthan, J.; Minet, O.; Helfmann, J.; Herrig, M.; Müller, G. The spatial variation of the refractive index in biological cells. *Phys. Med. Biol.* **1996**, *41*, 369–382. [CrossRef]
9. Rafelski, S.; Marshall, W. Building the cell: Design principles of cellular architecture. *Nat. Rev. Mol. Cell Biol.* **2008**, *9*, 593–602. [CrossRef]
10. Wiemerslage, L.; Lee, D. Quantification of mitochondrial morphology in neurites of dopaminergic neurons using multiple parameters. *J. Neurosci. Methods* **2016**, *15*, 56–65. [CrossRef]
11. Kulmaganbetov, M.; Bevan, R.J.; Anantrasirichai, N.; Achim, A.; Erchova, I.; White, N.; Albon, J.; Morgan, J.E. Textural Feature Analysis of Optical Coherence Tomography Phantoms. *Electronics* **2022**, *11*, 669. [CrossRef]
12. Kwon, I.H.; Kim, H.; Kim, D.Y.; Lee, H.; Lee, S. Utilizing Optical Phantoms for Biomedical-optics Technology: Recent Advances and Challenges. *Curr. Opt. Photon.* **2024**, *8*, 327–344. [CrossRef]
13. Zhang, T.; Yuan, S.; Xu, C.; Liu, P.; Chang, H.C.; Ng, S.H.C.; Ren, H.; Yuan, W. PneumaOCT: Pneumatic optical coherence tomography endoscopy for targeted distortion-free imaging in tortuous and narrow internal lumens. *Sci. Adv.* **2024**, *10*, eadp3145. [CrossRef] [PubMed]
14. Agrawal, A.; Lamont, A.C.; Liu, Z.; Sochol, R.; Hammer, D.X. Engineered Texture Phantom for Measuring Lateral Resolution of Adaptive Optics Ophthalmic Imaging Systems. In Proceedings of the Imaging and Applied Optics Congress, Vancouver, BC, Canada, 22–26 June 2020; OSA Technical Digest (Optica Publishing Group): Washington, DC, USA, 2020; Paper OTh5B.4. [CrossRef]
15. Quan, K.M.; Christison, G.B.; MacKenzie, H.A.; Hodgson, P. Glucose determination by a pulsed photoacoustic technique: An experimental study using a gelatin-based tissue phantom. *Phys. Med. Biol.* **1993**, *38*, 1911–1922. [CrossRef] [PubMed]
16. Pan, Y.; Birngruber, R.; Rosperich, J.; Engelhardt, R. Low-coherence optical tomography in turbid tissue: Theoretical analysis. *Appl. Opt.* **1995**, *34*, 6564–6574. [CrossRef]
17. Schmitt, J.M.; Lee, S.L.; Yung, K.M. An optical coherence microscope with enhanced resolving power in thick tissue. *Opt. Commun.* **1997**, *142*, 203–207. [CrossRef]
18. Cubeddu, R.; Pifferi, A.; Taroni, P.; Torricelli, A.; Valentini, G. A solid tissue phantom for photon migration studies. *Phys. Med. Biol.* **1997**, *42*, 1971–1979. [CrossRef]
19. Catheline, S.; Gennisson, J.L.; Delon, G.; Fink, M.; Sinkus, R.; Abouelkaram, S.; Culioli, J. Measuring of viscoelastic properties of homogeneous soft solid using transient elastography: An inverse problem approach. *J. Acoust. Soc. Am.* **2004**, *116*, 3734–3741. [CrossRef]
20. Brum, J.; Catheline, S.; Benech, N.; Negreira, C. Shear elasticity estimation from surface wave: The time reversal approach. *J. Acoust. Soc. Am.* **2008**, *124*, 3377–3380. [CrossRef]

21. Chen, S.; Urban, M.W.; Pislaru, C.; Kinnick, R.; Zheng, Y.; Yao, A.; Greenleaf, J.F. Shearwave dispersion ultrasound vibrometry (SDUV) for measuring tissue elasticity and viscosity. *IEEE Trans. Ultrason. Ferroelectr. Freq. Control.* **2009**, *56*, 55–62. [CrossRef]
22. Schmitt, J.M. OCT elastography: Imaging microscopic deformation and strain of tissue. *Opt. Exp.* **1998**, *3*, 199–211. [CrossRef]
23. Browne, J.E.; Ramnarine, K.V.; Watson, A.J.; Hoskins, P.R. Assessment of the acoustic properties of common tissue-mimicking test phantoms. *Ultrasound Med. Biol.* **2003**, *29*, 1053–1060. [CrossRef] [PubMed]
24. Zhang, X.; Qiang, B.; Greenleaf, J. Comparison of the surface wave method and the indentation method for measuring the elasticity of gelatin phantoms of different concentrations. *Ultrasonics* **2011**, *51*, 157–164. [CrossRef] [PubMed]
25. De Grand, A.M.; Lomnes, S.J.; Lee, D.S.; Pietrzykowski, M.; Ohnishi, S.; Morgan, T.G.; Gogbashian, A.; Laurence, R.G.; Frangioni, J.V. Tissue-like phantoms for near-infrared fluorescence imaging system assessment and the training of surgeons. *J. Biomed. Opt.* **2006**, *11*, 014007. [CrossRef]
26. Wagnières, G.; Cheng, S.; Zellweger, M.; Utke, N.; Braichotte, D.; Ballini, J.P.; van den Bergh, H. An optical phantom with tissue-like properties in the visible for use in PDT and fluorescence spectroscopy. *Phys. Med. Biol.* **1997**, *42*, 1415–1426. [CrossRef] [PubMed]
27. Esmonde-White, F.W.L.; Esmonde-White, K.A.; Kole, M.R.; Goldstein, S.A.; Roessler, B.J.; Morris, M.D. Biomedical tissue phantoms with controlled geometric and optical properties for Raman spectroscopy and tomography. *Analyst* **2011**, *136*, 4437–4446. [CrossRef]
28. Lamouche, G.; Kennedy, B.F.; Kennedy, K.M.; Bisaillon, C.E.; Curatolo, A.; Campbell, G.; Pazos, V.; Sampson, D.D. Review of tissue simulating phantoms with controllable optical, mechanical and structural properties for use in optical coherence tomography. *Biomed. Opt. Express* **2012**, *3*, 1381–1398. [CrossRef]
29. Madsen, E.L.; Hobson, M.A.; Shi, H.; Varghese, T.; Frank, G.R. Tissue-mimicking agar/gelatin materials for use in heterogeneous elastography phantoms. *Phys. Med. Biol.* **2005**, *50*, 5597–5618. [CrossRef]
30. Richardson, C.; Bernard, S.; Dinh, V.A. A Cost-effective, Gelatin-Based Phantom Model for Learning Ultrasound-Guided Fine-Needle Aspiration Procedures of the Head and Neck. *J. Ultrasound Med.* **2015**, *34*, 1479–1484. [CrossRef]
31. Bolin, F.P.; Preuss, L.E.; Taylor, R.C.; Ference, R.J. Refractive index of some mammalian tissues using a fiber optic cladding method. *Appl. Opt.* **1989**, *28*, 2297–2303. [CrossRef]
32. Bays, R.; Wagnières, G.; Robert, D.; Theumann, J.F.; Vitkin, A.; Savary, J.F.; Monnier, P.; van den Bergh, H. Three-dimensional optical phantom and its application in photodynamic therapy. *Lasers Surg. Med.* **1997**, *21*, 227–234. [CrossRef]
33. Williams, D.R. Visual consequences of the foveal pit. *Investig. Ophthalmol. Vis. Sci.* **1980**, *19*, 653–667.
34. Bisaillon, C.-E.; Lanthier, M.-M.; Dufour, M.L.; Lamouche, G. Durable coronary artery phantoms for optical coherence tomography. In Proceedings of the SPIE 7161, Photonic Therapeutics and Diagnostics V, San Jose, CA, USA, 24–29 January 2009; p. 71612E. [CrossRef]
35. Zoutenbier, V.S.; Amelink, A.; de Boer, J.F. Ex-corpus human blood flow system for flow and physiological control in retina-mimicking silicone phantoms. In Proceedings of the SPIE PC12147, Tissue Optics and Photonics II, Strasbourg, France, 3 April–23 May 2022; p. PC1214705.
36. Potlov, A.Y.; Frolov, S.V.; Proskurin, S.G. Tissue-mimicking phantoms of human retina with consideration to blood circulation for Doppler optical coherence tomography. In Proceedings of the SPIE 11457, Saratov Fall Meeting 2019: Optical and Nano-Technologies for Biology and Medicine, Saratov, Russia, 23–27 September 2019; p. 114571S. [CrossRef]
37. Ayers, F.; Grant, A.; Kuo, D.; Cuccia, D.J.; Durkin, A.J. Fabrication and characterization of silicone-based tissue phantoms with tunable optical properties in the visible and near infrared domain. In Proceedings of the SPIE 6870, Design and Performance Validation of Phantoms Used in Conjunction with Optical Measurements of Tissue, San Jose, CA, USA, 19–21 January 2008; p. 687007. [CrossRef]
38. Long, R.; King, T.; Akl, T.; Ericson, M.N.; Wilson, M.; Coté, G.L.; McShane, M.J. Optofluidic phantom mimicking optical properties of porcine livers. *Biomed. Opt. Exp.* **2011**, *2*, 1877–1892. [CrossRef] [PubMed]
39. Avigo, C.; Di Lascio, N.; Armanetti, P.; Kusmic, C.; Cavigli, L.; Ratto, F.; Meucci, S.; Masciullo, C.; Cecchini, M.; Pini, R.; et al. Organosilicon phantom for photoacoustic imaging. *J. Biomed. Opt.* **2015**, *20*, 046008. [CrossRef] [PubMed]
40. Bohndiek, S.E.; Bodapati, S.; Van De Sompel, D.; Kothapalli, S.R.; Gambhir, S.S. Development and application of stable phantoms for the evaluation of photoacoustic imaging instruments. *PLoS ONE* **2013**, *8*, e75533. [CrossRef]
41. Zell, K.; Sperl, J.I.; Vogel, M.W.; Niessner, R.; Haisch, C. Acoustical properties of selected tissue phantom materials for ultrasound imaging. *Phys. Med. Biol.* **2007**, *52*, N475–N484. [CrossRef]
42. Wu, Q.; Ren, W.; Yu, Z.; Dong, E.; Zhang, S.; Xu, R.X. Microfabrication of polydimethylsiloxane phantoms to simulate tumor hypoxia and vascular anomaly. *J. Biomed. Opt.* **2015**, *20*, 121308. [CrossRef]
43. Saager, R.B.; Kondru, C.; Au, K.; Sry, K.; Ayers, F.; Durkin, A.J. Multilayer silicone phantoms for the evaluation of quantitative optical techniques in skin imaging. In Proceedings of the SPIE 7567, Design and Performance Validation of Phantoms Used in Conjunction with Optical Measurement of Tissue II, San Jose, CA, USA, 23–28 January 2010; p. 756706. [CrossRef]

44. Wang, H.; Liu, W.; Hu, Z.; Li, X.; Li, F.; Duan, L. Model eye tool for retinal optical coherence tomography instrument calibration. *J. Innov. Opt. Health Sci.* **2021**, *14*, 2150010. [CrossRef]
45. Al-Sadiq, H.; Walters, J.; Alshayeb, A.; Parekh, H.; Veidt, M. Tissue mimicking phantom of the acoustical and geometrical properties of the human eye. In Proceedings of the Conference of the Acoustical Society of New Zealand, Wellington, New Zealand, 31 October–2 November 2022.
46. Chang, S.; Handwerker, J.; Giannico, G.A.; Chang, S.S.; Bowden, A.K. Birefringent tissue-mimicking phantom for polarization-sensitive optical coherence tomography imaging. *J. Biomed. Opt.* **2022**, *27*, 074711. [CrossRef]
47. Fromageau, J.; Brusseau, E.; Vray, D.; Gimenez, G.; Delachartre, P. Characterization of PVA cryogel for intravascular ultrasound elasticity imaging. *IEEE Trans. Ultrason. Ferroelectr. Freq. Control.* **2003**, *50*, 1318–1324. [CrossRef]
48. Mano, I.; Goshima, H.; Nambu, M.; Iio, M. New polyvinyl alcohol gel material for MRI phantoms. *Magn. Reson. Med.* **1986**, *3*, 921–926. [CrossRef]
49. Chu, K.C.; Rutt, B.K. Polyvinyl alcohol cryogel: An ideal phantom material for MR studies of arterial flow and elasticity. *Magn. Reson. Med.* **1997**, *37*, 314–319. [CrossRef] [PubMed]
50. Brusseau, E.; Fromageau, J.; Finet, G.; Delachartre, P.; Vray, D. Axial strain imaging of intravascular data: Results on polyvinyl alcohol cryogel phantoms and carotid artery. *Ultrasound Med. Biol.* **2001**, *27*, 1631–1642. [CrossRef] [PubMed]
51. Surry, K.J.; Austin, H.J.; Fenster, A.; Peters, T.M. Poly(vinyl alcohol) cryogel phantoms for use in ultrasound and MR imaging. *Phys. Med. Biol.* **2004**, *49*, 5529–5546. [CrossRef] [PubMed]
52. Kharine, A.; Manohar, S.; Seeton, R.; Kolkman, R.G.; Bolt, R.A.; Steenbergen, W.; de Mul, F.F. Poly(vinyl alcohol) gels for use as tissue phantoms in photoacoustic mammography. *Phys. Med. Biol.* **2003**, *48*, 357–370. [CrossRef]
53. Fogli, G.; Orsi, G.; De Maria, C.; Montemurro, F.; Palla, M.; Rizzo, S.; Vozzi, G. New eye phantom for ophthalmic surgery. *J. Biomed. Opt.* **2014**, *19*, 068001. [CrossRef]
54. Kaetsu, H.; Uchida, T.; Shinya, N. Increased effectiveness of fibrin sealant with a higher fibrin concentration. *Int. J. Adhes. Adhes.* **2000**, *20*, 27–31. [CrossRef]
55. Göbel, K.; Eichler, S.; Wiendl, H.; Chavakis, T.; Kleinschnitz, C.; Meuth, S.G. The Coagulation Factors Fibrinogen, Thrombin, and Factor XII in Inflammatory Disorders—A Systematic Review. *Front. Immunol.* **2018**, *9*, 1731. [CrossRef]
56. Kennedy, B.F.; Loitsch, S.; McLaughlin, R.A.; Scolaro, L.; Rigby, P.; Sampson, D.D. Fibrin phantom for use in optical coherence tomography. *J. Biomed. Opt.* **2010**, *15*, 030507. [CrossRef]
57. Yu, H.; Jang, J.; Lim, J.; Park, J.H.; Jang, W.; Kim, J.Y.; Park, Y. Depth-enhanced 2-D optical coherence tomography using complex wavefront shaping. *Opt. Exp.* **2014**, *22*, 7514–7523. [CrossRef]
58. Kim, M.; Im, S.; Park, I.; Kim, D.; Kim, E.S.; Joseph, J.; Yoon, J. Fabrication of agar-based tissue-mimicking phantom for the technical evaluation of biomedical optical imaging systems. *Curr. Appl. Phys.* **2024**, *61*, 80–85. [CrossRef]
59. Khasawneh, A.; Kuroda, M.; Yoshimura, Y.; Sugianto, I.; Bamgbose, B.O.; Hamada, K.; Barham, M.; Tekiki, N.; Konishi, K.; Sugimoto, K.; et al. Development of a novel phantom using polyethylene glycol for the visualization of restricted diffusion in diffusion kurtosis imaging and apparent diffusion coefficient subtraction method. *Biomed. Rep.* **2020**, *13*, 52. [CrossRef]
60. Nanda Kumar, Y.; Singh, Z.; Wang, Y.N.; Schade, G.R.; Kreider, W.; Bruce, M.; Vlaisavljevich, E.; Khokhlova, T.D.; Maxwell, A.D. Development of Tough Hydrogel Phantoms to Mimic Fibrous Tissue for Focused Ultrasound Therapies. *Ultrasound Med. Bio.* **2022**, *48*, 1762–1777. [CrossRef] [PubMed]
61. Qiu, H.; Nazarenus, J.; Egeler, B.; Thode, T.; Osman, F.; Osmonov, D.; Bahr, J.; Kaps, S.; Siebert, F.A.; Koch, R.; et al. Hydrogel System with Independent Tailoring of Mechanics, CT, and US Contrasts for Affordable Medical Phantoms. *ACS Mater. Lett.* **2024**, *6*, 4847–4853. [CrossRef]
62. Malektaj, H.; Drozdov, A.D.; deClaville Christiansen, J. Mechanical Properties of Alginate Hydrogels Cross-Linked with Multivalent Cations. *Polymers* **2023**, *15*, 3012. [CrossRef]
63. Delpy, D.T.; Cope, M.; van der Zee, P.; Arridge, S.; Wray, S.; Wyatt, J. Estimation of optical pathlength through tissue from direct time of flight measurement. *Phys. Med. Biol.* **1988**, *33*, 1433–1442. [CrossRef] [PubMed]
64. Al Rawashdeh, W.; Kray, S.; Pich, A.; Pargen, S.; Balaceanu, A.; Lenz, M.; Spöler, F.; Kiessling, F.; Lederle, W. Polymeric nanoparticles as OCT contrast agents. *J. Nanopart. Res.* **2012**, *14*, 1255. [CrossRef]
65. Chang, R.C.; Johnson, P.; Stafford, C.M.; Hwang, J. Fabrication and characterization of a multilayered optical tissue model with embedded scattering microspheres in polymeric materials. *Biomed. Opt. Exp.* **2012**, *3*, 1326–1339. [CrossRef]
66. Bao, Y.; Huang, Y.; Li, W.; Zhu, K. Comparison of the scattering properties between TiO_2 and ITO clusters based on the particle superposition model. *Opt. Mater. Express* **2019**, *9*, 562–575. [CrossRef]
67. Curatolo, A.; Kennedy, B.F.; Sampson, D.D. Structured three-dimensional optical phantom for optical coherence tomography. *Opt. Exp.* **2011**, *19*, 19480–19485. [CrossRef]
68. Liba, O.; Lew, M.D.; SoRelle, E.D.; Dutta, R.; Sen, D.; Moshfeghi, D.M.; Chu, S.; de la Zerda, A. Speckle-modulating optical coherence tomography in living mice and humans. *Nat. Commun.* **2017**, *8*, 15845. [CrossRef] [PubMed]

69. Corcoran, A.; Muyo, G.; van Hemert, J.; Gorman, A.; Harvey, A.R. Application of a wide-field phantom eye for optical coherence tomography and reflectance imaging. *J. Mod. Opt.* **2015**, *62*, 1828–1838. [CrossRef] [PubMed]
70. Lee, H.J.; Samiudin, N.M.; Lee, T.G.; Doh, I.; Lee, S.W. Retina phantom for the evaluation of optical coherence tomography angiography based on microfluidic channels. *Biomed. Opt. Express* **2019**, *10*, 5535–5548. [CrossRef] [PubMed]
71. Lamont, A.C.; Restaino, M.A.; Alsharhan, A.T.; Liu, Z.; Hammer, D.X.; Sochol, R.D.; Agrawal, A. Direct laser writing of a titanium dioxide-laden retinal cone phantom for adaptive optics-optical coherence tomography. *Opt. Mater. Express* **2020**, *10*, 2757–2767. [CrossRef]
72. Kuttippurath, V.; Slijkhuis, N.; Liu, S.; van Soest, G. Spectroscopic optical coherence tomography at 1200 nm for lipid detection. *J. Biomed. Opt.* **2023**, *28*, 096002. [CrossRef]
73. Motipally, S.I.; Kolson, D.R.; Guan, T.; Kolandaivelu, S. Aberrant lipid accumulation and retinal pigmental epithelium dysfunction in PRCD-deficient mice. *Exp. Eye Res.* **2024**, *246*, 110016. [CrossRef]
74. Philipp, H.R.; Taft, E.A. Optical Constants of Silicon in the Region 1 to 10 ev. *Phys. Rev.* **1960**, *120*, 37–38. [CrossRef]
75. Bisaillon, C.-E.; Lamouche, G.; Maciejko, R.; Dufour, M.; Monchalin, J.P. Deformable and durable phantoms with controlled density of scatterers. *Phys. Med. Biol.* **2008**, *53*, N237–N247. [CrossRef]
76. Ki, J.; Lee, H.; Lee, T.G.; Lee, S.W.; Wi, J.S.; Na, H.K. Visualization Materials Using Silicon-Based Optical Nanodisks (ViSiON) for Enhanced NIR Imaging in Ophthalmology. *Adv. Healthc. Mater.* **2024**, *13*, e2303713. [CrossRef]
77. Zabotnov, S.V.; Kashaev, F.V.; Shuleiko, D.V.; Gongalsky, M.B.; Golovan, L.A.; Kashkarov, P.K.; Loginova, D.A.; Agrba, P.D.; Sergeeva, E.A.; Kirillin, M.Y. Silicon nanoparticles as contrast agents in the methods of optical biomedical diagnostics. *Quantum Electron.* **2017**, *47*, 638–646. [CrossRef]
78. Loo, C.; Lin, A.; Hirsch, L.; Lee, M.H.; Barton, J.; Halas, N.; West, J.; Drezek, R. Nanoshell-enabled photonics-based imaging and therapy of cancer. *Technol. Cancer Res. Treat.* **2004**, *3*, 33–40. [CrossRef] [PubMed]
79. Tuersun, P.; Han, X.; Ren, K.F. Backscattering Properties of Gold Nanoshells: Quantitative Analysis and Optimization for Biological Imaging. *Procedia Eng.* **2015**, *102*, 1511–1519. [CrossRef]
80. Agrawal, A.; Huang, S.; Wei Haw Lin, A.; Lee, M.H.; Barton, J.K.; Drezek, R.A.; Pfefer, T.J. Quantitative evaluation of optical coherence tomography signal enhancement with gold nanoshells. *J. Biomed. Opt.* **2006**, *11*, 041121. [CrossRef] [PubMed]
81. Kah, J.C.; Chow, T.H.; Ng, B.K.; Razul, S.G.; Olivo, M.; Sheppard, C.J. Concentration dependence of gold nanoshells on the enhancement of optical coherence tomography images: A quantitative study. *Appl. Opt.* **2009**, *48*, D96–D108. [CrossRef]
82. Zagaynova, E.V.; Shirmanova, M.V.; Kirillin, M.Y.; Khlebtsov, B.N.; Orlova, A.G.; Balalaeva, I.V.; Sirotkina, M.A.; Bugrova, M.L.; Agrba, P.D.; Kamensky, V.A. Contrasting properties of gold nanoparticles for optical coherence tomography: Phantom, in vivo studies and Monte Carlo simulation. *Phys. Med. Biol.* **2008**, *53*, 4995–5009. [CrossRef]
83. Min-Ho, L.; Nammalvar, V.; Gobin, A.; Barton, J.; West, J.; Drezek, R. Nanoshells as contrast agents for scatter-based optical imaging. In Proceedings of the 3rd IEEE International Symposium on Biomedical Imaging: Nano to Macro, Arlington, WA, USA, 6–9 April 2006; pp. 371–374. [CrossRef]
84. Guo, L.; Zhao, Q.; Wang, M. Core–Shell Microspheres with Encapsulated Gold Nanoparticle Carriers for Controlled Release of Anti-Cancer Drugs. *J. Funct. Biomater.* **2024**, *15*, 277. [CrossRef]
85. Wilczyński, T.; Zalejska-Fiolka, J.; Sapeta-Wieckowska, S.; Sarnat-Kucharczyk, M.; Rokicki, W. In situ oxidative stress in patients with epiretinal membrane. *Acta Biochim. Pol.* **2024**, *71*, 13581. [CrossRef]
86. Wang, T.; Song, Y.; Bell, B.A.; Anderson, B.D.; Lee, T.T.; Yu, W.; Dunaief, J.L. Complement C3 knockout protects photoreceptors in the sodium iodate model. *Exp. Eye Res.* **2025**, *250*, 110161. [CrossRef] [PubMed]
87. Han, J.; Chear, S.; Talbot, J.; Swier, V.; Booth, C.; Reuben-Thomas, C.; Dalvi, S.; Weimer, J.M.; Hewitt, A.W.; Cook, A.L.; et al. Genetic and Cellular Basis of Impaired Phagocytosis and Photoreceptor Degeneration in CLN3 Disease. *Investig. Ophthalmol. Vis. Sci.* **2024**, *65*, 23. [CrossRef]
88. Olufsen, M.E.; Hannibal, J.; Sørensen, N.B.; Christiansen, A.T.; Christensen, U.; Pertile, G.; Steel, D.H.; Heegaard, S.; Kiilgaard, J.F. Wound Healing in a Porcine Model of Retinal Holes. *Investig. Ophthalmol. Vis. Sci.* **2024**, *65*, 35. [CrossRef]
89. Peng, N.; Xu, C.; Shen, Y.; Yuan, W.; Yang, X.; Qi, C.; Qiu, H.; Gu, Y.; Chen, D. Accurate attenuation characterization in optical coherence tomography using multi-reference phantoms and deep learning. *Biomed. Opt. Express* **2024**, *15*, 6697–6714. [CrossRef] [PubMed]
90. Heikka, T.; Ometto, G.; Montesano, G.; Rowe, S.; Jansonius, N.M.; Crabb, D.P. Testing a phantom eye under various signal-to-noise ratio conditions using eleven different OCT devices. *Biomed. Opt. Express* **2020**, *11*, 1306–1315. [CrossRef] [PubMed]
91. Zakir, R.; Iqbal, K.; Hassaan Ali, M.; Tariq Mirza, U.; Mahmood, K.; Riaz, S.; Hashmani, N. The outcomes and usefulness of Intraoperative Optical Coherence Tomography in vitreoretinal surgery and its impact on surgical decision making. *Rom. J. Ophthalmol.* **2022**, *66*, 55–60. [CrossRef] [PubMed]
92. Toygar, O.; Riemann, C. Intraoperative optical coherence tomography in macula involving rhegmatogenous retinal detachment repair with pars plana vitrectomy and perfluoron. *Eye* **2016**, *30*, 23–30. [CrossRef]

93. Borrelli, E.; Palmieri, M.; Aharrh-Gnama, A.; Ciciarelli, V.; Mastropasqua, R.; Carpineto, P. Intraoperative optical coherence tomography in the full-thickness macular hole surgery with internal limiting membrane inverted flap placement. *Int. Ophthalmol.* **2019**, *39*, 929–934. [CrossRef]
94. Hwang, J.; Goldfain, A.M.; Zhang, H.; Briggman, K. Material Characterization of Phantom Standards Developed by NIST for Quantitative Optical Medical Imaging Applications. Available online: https://cormusa.org/wp-content/uploads/2024/01/1-CORM2023-OPM-Hwang.pdf (accessed on 1 April 2025).
95. Kulmaganbetov, M.; Bevan, R.; Want, A.; Anantrasirichai, N.; Achim, A.; Albon, J.; Morgan, J. SVM-Based Optical Detection of Retinal Ganglion Cell Apoptosis. *Photonics* **2025**, *12*, 128. [CrossRef]
96. Kulmaganbetov, M.; Morgan, J.E. Application of Texture Analysis in Retinal OCT Imaging. In *Handbook of Texture Analysis*; CRC Press: Boca Raton, FL, USA, 2024; pp. 154–179.
97. Inkarbekov, M.; Kulmaganbetov, M.; Bazarbekova, G.; Baiyrkhanova, A. Assessment of Postoperative Retinal Complications and the Possibility of Optical Diagnostics Using Support Vector Machine. *Salud Cienc. Tecnol.* **2024**, *4*, 1359. [CrossRef]